Journal of Catalysis 367 (2018) 7–15

Contents lists available at ScienceDirect

Journal of Catalysis

journal homepage: www.elsevier.com/locate/jcat

On the deactivation mechanism of zeolite catalyst in ethanol to butadiene conversion

Tingting Yan [a], Liu Yang [a], Weili Dai [a,c,*], Chuanming Wang [d], Guangjun Wu [a,b], Naijia Guan [a,b], Michael Hunger [c], Landong Li [a,b,*]

[a] School of Materials Science and Engineering & National Institute for Advanced Materials, Nankai University, Tianjin 300350, PR China
[b] Key Laboratory of Advanced Energy Materials Chemistry of the Ministry of Education, Collaborative Innovation Center of Chemical Science and Engineering, Nankai University, Tianjin 300071, PR China
[c] Institute of Chemical Technology, University of Stuttgart, 70550 Stuttgart, Germany
[d] State Key Laboratory of Green Chemical Engineering and Industrial Catalysis, SINOPEC Shanghai Research Institute of Petrochemical Technology, Shanghai 201208, PR China

ARTICLE INFO

Article history:
Received 12 June 2018
Revised 18 August 2018
Accepted 22 August 2018

Keywords:
Ethanol to butadiene
Deactivation mechanism
Zn-Y/Beta zeolite
Spectroscopy
Unsaturated aldehydes/ketones

ABSTRACT

Despite of extensive attention on the ethanol to butadiene (ETB) conversion, the catalyst deactivation during ETB conversion is rarely investigated and poorly understood. Here, the mechanism of the catalyst deactivation during the ETB conversion over Zn-Y/Beta was investigated through several complementary approaches, including XPS, TGA, GC–MS, *in situ* DRIFTS, UV–vis and ^{13}C CP MAS NMR spectroscopy. Acetaldehyde was observed to be the first reactive intermediate formed in the ETB conversion, which was rapidly involved in a subsequent aldol condensation with the simultaneous production of acetone. Due to a self- and cross-condensation of acetaldehyde and acetone, long chain unsaturated aldehydes/ketones were formed and further converted to 2,4-dimethyl benzaldehyde via a cyclization reaction, which could gradually cover the active sites and led to catalyst deactivation. Fortunately, the deactivating species could be removed from catalyst surface via simple calcination and the complete regeneration of Zn-Y/Beta could be realized.

1. Introduction

Growing concerns regarding environment deterioration and the gradual depletion of fossil resources become a key driving force for the sustainable production of important chemicals [1]. Bioethanol obtained from the fermentation of sugars and starch is regarded as a most attractive renewable material to produce basic chemicals like acetaldehyde, acetic acid, isobutene, and butadiene [2–4]. In particular, the conversion of ethanol to butadiene (ETB) is becoming an attractive route since butadiene is an important monomer for the production of polymers and polymer intermediates [1]. The bioethanol-based route to butadiene possesses an apparent advantage over the traditional naphtha-based one according to the techno-economic analysis, life-cycle assessment, and green chemistry principles [5].

Recently, extensive attention has been focused on the ETB conversion. The reaction mechanism and network of the ETB conversion have been extensively investigated [6–11], and several key reaction steps are now generally accepted, including (i) the dehydrogenation of ethanol to acetaldehyde, (ii) the aldol condensation of acetaldehyde to acetaldol, (iii) the dehydration of acetaldol to crotonaldehyde, (iv) the Meerwein-Ponndorf-Verley reduction of crotonaldehyde to crotonyl alcohol, and (v) the dehydration of crotonyl alcohol to butadiene [3,12]. On the other hand, a variety of catalysts have been explored to achieve high butadiene yield and productivity in ETB conversion. In the most cases, mixed metal oxides are studied as candidating catalysts, such as doped magnesia-silica catalysts prepared via different procedures [4,13–28]. Moreover, with addition of metal or metal oxides to Lewis acidic catalysts, e.g. zeolite Zr-Beta or ZrO_2/SiO_2, the two-step ETB catalysts could be transferred into one-step ETB catalysts, and the butadiene yields could be significantly promoted [9,29–37]. Our recent work indicates that Zn–Y/Beta zeolite containing dehydrogenation, condensation and Lewis acid sites exhibits a remarkable ETB activity, and a state-of-the-art butadiene productivity of 2.33 $g_{Butadiene}/g_{Cat}/h$ with butadiene selectivity of 63% could be obtained by well balancing the different types of active sites [12,38]. Despite of the significant achievements made so far, the catalyst stability remains a key problem for the long-running of the ETB conversion and the reasons for

* Corresponding authors at: School of Materials Science and Engineering & National Institute for Advanced Materials, Nankai University, Tianjin 300350, PR China.
E-mail addresses: weilidai@nankai.edu.cn (W. Dai), lild@nankai.edu.cn (L. Li).

https://doi.org/10.1016/j.jcat.2018.08.019
0021-9517/

catalyst deactivation are not understood yet. An improved knowledge on the detailed deactivation mechanism of an ETB catalyst is essential for its industrial application [1], and, therefore, the main goal of the present work.

In this work, Zn- and Y-modified zeolite Beta was utilized as a model catalyst for investigating the deactivation mechanism during the ETB conversion. The catalytic performance of the zeolite Zn-Y/Beta in the ETB conversion for a time-on-stream of up to 70 h was evaluated on a fixed-bed reactor. The intermediary products formed during the initial stages of the ETB conversion were monitored by on-line MS, while the reactive intermediates formed during the whole process of the ETB conversion were investigated by *in situ* DRIFTS and UV–vis spectroscopy. Moreover, the physicochemical properties of the catalysts before and after ETB conversion were analyzed by XRD, nitrogen physisorption, and XPS. The organic deposits occluded in the zeolite catalyst as a result of the ETB conversion were determined by TGA, GC–MS, and ^{13}C CP MAS NMR spectroscopy. According to the catalytic performance of the Zn-Y/Beta zeolite and the spectroscopic results, the deactivation behaviors of this catalyst were disclosed, and the deactivation mechanism was discussed in detail. The methodology employed here can be extended to the other cascade heterogeneous catalytic reactions.

2. Experimental section

2.1. Catalyst preparation

The Zn-Y/Beta zeolite was prepared via a two-step metallation procedure [38]. First, the dealuminated zeolite Si-Beta was obtained by treating the commercial H-Beta zeolite (n_{Si}/n_{Al} = 13.5, Sinopec Co.) in 13 mol/L nitric acid aqueous solution. Afterwards, zinc and yttrium were introduced to Si-Beta by mixing Si-Beta with desired amounts of zinc and yttrium nitrates, followed by calcination in flowing air at 823 K for 6 h. The final product 5% Zn-5%Y/Beta (5% refers to the weight loading), hereinafter abbreviated as Zn-Y/Beta, was directly utilized as a solid catalyst in the ETB conversion.

2.2. Catalyst evaluation

The ETB conversion was performed in a fixed-bed reactor at atmospheric pressure as described in our previous work [12]. In a typical experiment, 0.3 g of the Zn-Y/Beta catalyst (sieve fraction, 0.25–0.5 mm) was placed in a fixed-bed reactor and treated in flowing He (20 mL/min) at 723 K for 1 h. After cooling down to 623 K, ethanol was introduced into the reactor utilizing a Shimadzu LC-2AT Dual Reciprocating Plunger HPLC pump at the rate of 0.5 mL/h. After the ETB reaction, the catalyst was regenerated by calcination in flowing air (20 mL/min) at 823 K for 6 h. The reaction products were analyzed by an on-line gas chromatograph (Shimadzu GC-2010 plus) with a Poraplot Q-HT column (40 m × 0.18 mm × 0.18 μm) and a flame ionization detector (FID).

To get more information about the main reaction products formed during the ETB conversion, the fixed-bed reactor was also connected with a downstream gas sampling mass spectrometer (MS, Pfeiffer Omnistar).

2.3. Characterization of the fresh and spent Zn-Y/Beta catalysts

The X-ray diffraction (XRD) patterns of the fresh and spent catalysts were recorded on a Rigaku SmartLab powder diffractometer using Cu-Kα radiation (λ = 1.5418 Å) with a scanning rate of 5°/min in the range of 2θ = 5–50°.

The surface areas and pore volumes of the fresh and spent catalysts were measured by means of nitrogen sorption on a Quantachrome iQ-MP gas adsorption analyzer at 77 K. Before the nitrogen adsorption, samples were dehydrated at 573 K for 6 h. The total surface area was calculated via the Brunauer-Emmett-Teller (BET) equation while the micropore volume was determined using the t-plot method.

X-ray photoelectron spectra (XPS) of the fresh and spent catalysts were recorded on a Thermo Scientific ESCALAB 250Xi spectrometer using a monochromatic Al-Kα X-ray source (hν = 1486.6 eV) as the excitation source. High-resolution spectra were recorded by using an aperture slot of 300 × 700 μm. The binding energies (±0.1 eV) were determined with respect to the position of the C 1s peak at 284.8 eV.

2.4. In situ DRIFTS and UV–vis studies of the ETB conversion over the Zn-Y/Beta catalyst

The nature of organic intermediates formed during the ETB conversion was *in situ* monitored by DRIFTS, and UV–vis spectroscopy as described in Ref. [39] and [40], respectively. DRIFT spectra were recorded on a Bruker Tensor 27 spectrometer equipped with a liquid N_2 cooled high sensitivity MCT detector and an *in situ* reaction chamber. About 20 mg of the catalyst powder was placed in the reaction chamber. Before starting the reaction, the catalysts were activated under flowing He (10 mL/min) at 723 K for 1 h. Subsequently, the temperature was decreased to 623 K for collecting the DRIFT background spectra. Afterwards, the ethanol was injected into the chamber at the constant rate of 0.025 mL/h (WHSV = 1.0 h^{-1}) and the *in situ* DRIFT spectra were recorded with a resolution of 4 cm^{-1} and an accumulation of 128 scans.

UV–vis spectra were recorded via an AvaSpec-2048 Fiber Optic spectrometer using an AvaLight-DH-S deuterium light source by Avantes and a glass fiber reflection probe HPSUV1000A by Oxford Electronics. Before the ETB reaction, the glass fiber reflection probe was placed in the fixed-bed reactor on the top of the catalyst with a gap of ca. 1.0 mm. Reference UV–vis spectra of the catalysts were recorded at reaction temperature prior to starting the ethanol injection. *In situ* UV–vis spectra were recorded in the diffuse reflection mode and over a spectral range of 200–600 nm [40].

2.5. TGA, GC–MS analysis, and ^{13}C CP MAS NMR investigations of organic deposits on spent Zn-Y/Beta catalysts

The amounts of entrapped organic species on the Zn-Y/Beta catalysts after the ETB reaction for different time-on-stream (TOS) were analyzed by TGA using a Setram Setsys 16/18 thermogravmetric analyzer. Typically, 0.1 g of spent catalyst was placed in an Al_2O_3 crucible and heated at the constant rate of 10 K/min in flowing O_2/Ar (20 vol%/80 vol%, 30 mL/min).

The nature of occluded organic compounds in the catalysts after the ETB reaction with different TOS was analyzed by GC–MS and ^{13}C CP MAS NMR spectroscopy. For GC–MS analysis, 0.1 g of the spent catalyst sample was carefully dissolved in 1 M HF solution. This solution was treated with CH_2Cl_2 to extract the organic compounds and the residual water was removed by the addition of sufficient sodium sulfate solid. Then, 0.2 μL of the organic extract were analyzed by GC–MS (GCMS-QP2010 SE) with a RXI-5MS column (30 m, 0.25 mm i.d., stationary phase thickness 0.25 μm). The following temperature program was employed: Isothermal heating at 313 K for 6 min, heating to 553 K with a rate of 10 K/min, and isothermal heating at 553 K for 10 min.

^{13}C CP MAS NMR measurements were performed on a Bruker Avance III 400WB spectrometer at the resonance frequency of 100.6 MHz, with cross polarization of 4 ms, the repetition time of 4 s, and the sample spinning rate of 8.0 kHz. To avoid contact with

air, all spent catalyst samples were transferred from the reactor into the gas-tight MAS NMR rotors inside a glove box purged with dry nitrogen gas.

3. Result and discussion

3.1. Catalytic performance of the Zn-Y/Beta catalyst in the ETB conversion

For introducing a novel heterogeneously catalyzed reaction in chemical industry, a stable performance of the catalyst is a key prerequisite. Therefore, the present work focus on the stability and regeneration ability of the Zn-Y/Beta catalyst in the ETB conversion. Zeolite deAl-Beta exclusively containing weakly acidic silanol groups was applied as support material. As shown in Fig. S1, ethene and diethyl ether (DEE) are the dominant products over deAl-Beta zeolite during the ethanol conversion. With increasing ethanol conversion, ethene selectivity increases, accompanied by the decline in DEE selectivity. These observations confirm that the silanol groups are responsible for ethanol dehydration to ethene or DEE. After Zn and Y introduction, butadiene and acetaldehyde became the dominant products, but a gradual deactivation occurred with the progress of the ETB conversion (Fig. 1). The ethanol conversion decreased from the initial 95.8% to about 40% at the TOS of 70 h. Simultaneously, the selectivity to butadiene gradually decreased from 71.4% to 32.1%, while the selectivity to acetaldehyde increased from 1.0% to 21.5%. Our previous studies indicated that the reaction mechanism of the ETB conversion over the bifunctional zeolite Zn-Y/Beta contains several steps, i.e. ethanol dehydrogenation, aldol condensation, Meerwein-Ponndorf-Verley reduction, and dehydration [12]. It indicated that the active sites of the Zn-Y/Beta catalyst for the further conversion of acetaldehyde to butadiene were gradually covered or blocked with the progress of the ETB conversion. On the other hand, the selectivity to ethene and diethyl ether (DEE) was nearly not changed. It indicated that the weak acidic sites, e.g. Si—OH groups, being active sites for the ethanol dehydration to ethene or DEE, were kept accessible during the ETB reaction. Furthermore, the ethene conversion over zeolite Zn-Y/Beta was also investigated at 623 K, but neglectable ethene conversion could be obtained (Fig. S2), excluding the sequential reaction of ethene and DEE to butadiene.

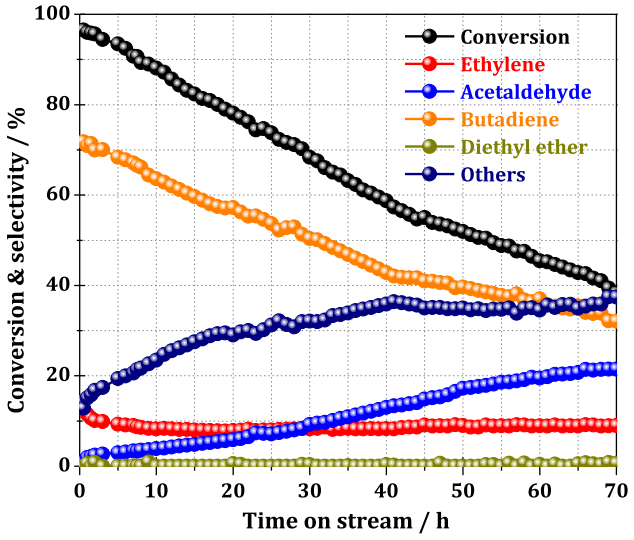

Fig. 1. Ethanol conversion and product selectivities during the ETB conversion over the Zn-Y/Beta catalyst under study at 673 K for TOS of up to 70 h, WHSV = 1.0^{-1}.

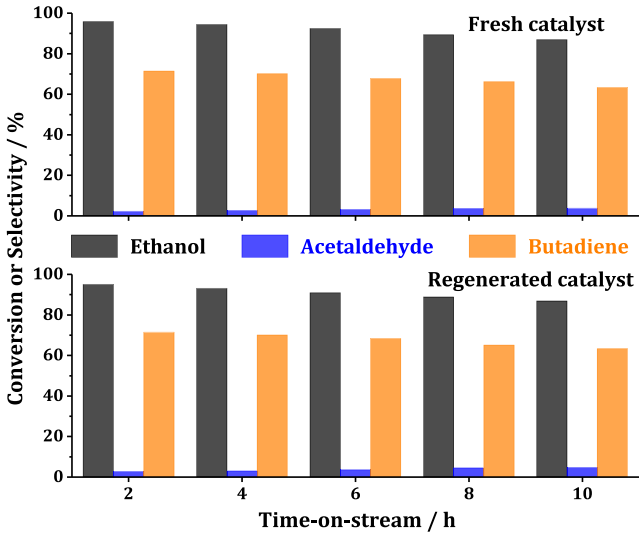

Fig. 2. Catalytic properties of regenerated Zn-Y/Beta catalyst after the ETB conversion at 673 K for TOS of up to 10 h, WHSV = 1.0^{-1}.

The regeneration ability of the spent Zn-Y/Beta catalyst after reaction for a time-on-stream of 70 h was investigated by calcination in air at 873 K for 6 h. As shown in Fig. 2, the catalytic performance could be fully recovered after regeneration of the spent Zn-Y/Beta catalyst, revealing that carbon deposits were responsible for the catalyst deactivation.

3.2. Physicochemical properties of the fresh and spent Zn-Y/Beta catalysts

For a better understanding of the change of the textual properties of the Zn-Y/Beta catalyst after the ETB conversion, the XRD patterns, BET surface areas, micropore volumes, and Zn and Y states of the catalysts before and after the reaction were investigated. As shown in Fig. S3, typical diffraction peaks characteristic of the BEA topology could be observed for both the fresh and the spent Zn-Y/Beta catalysts, revealing that the framework structure of zeolite Beta was well preserved after the ETB conversion, and the catalyst deactivation was not caused by the destroy of zeolite structure. This could be further confirmed by the similar adsorption/desorption isotherms in nitrogen physisorption for the fresh and spent Zn-Y/Beta catalysts (Fig. 3a). However, in comparison with the fresh sample, the surface area and micropore volume of the spent catalyst decreased to some extent, which should be due to the partial block of the micropores by the organic deposits.

To investigate the effect of coke compounds and hydrogen formed during the ETB conversion on the existing states of the Zn and Y species, XPS analysis of the fresh and spent Zn-Y/Beta catalysts were further performed. As shown in Fig. 3b, two same binding energy values of 160.9 and 159.0 eV corresponding to Y $3d_{3/2}$ and $3d_{5/2}$, respectively, were observed for both fresh and spent Zn-Y/Beta catalysts. According to our previous study [38], the higher values of Zn-Y/Beta zeolites compared to those of bulk Y_2O_3 are due to the formation of Si—O—Y bonds, which was not influenced by the coke compounds, indicating that the coke compounds and hydrogen formed during the ETB conversion have no influence on the valence states of Y species. Similarly, the Zn states were also not changed after the ETB conversion (Fig. 3c). However, a slight decrease of the Zn and Y signals occurred for the spent Zn-Y/Beta catalyst, hinting to the partial coverage or blocking of the Zn and Y species by coke compounds, in line with the previous studies

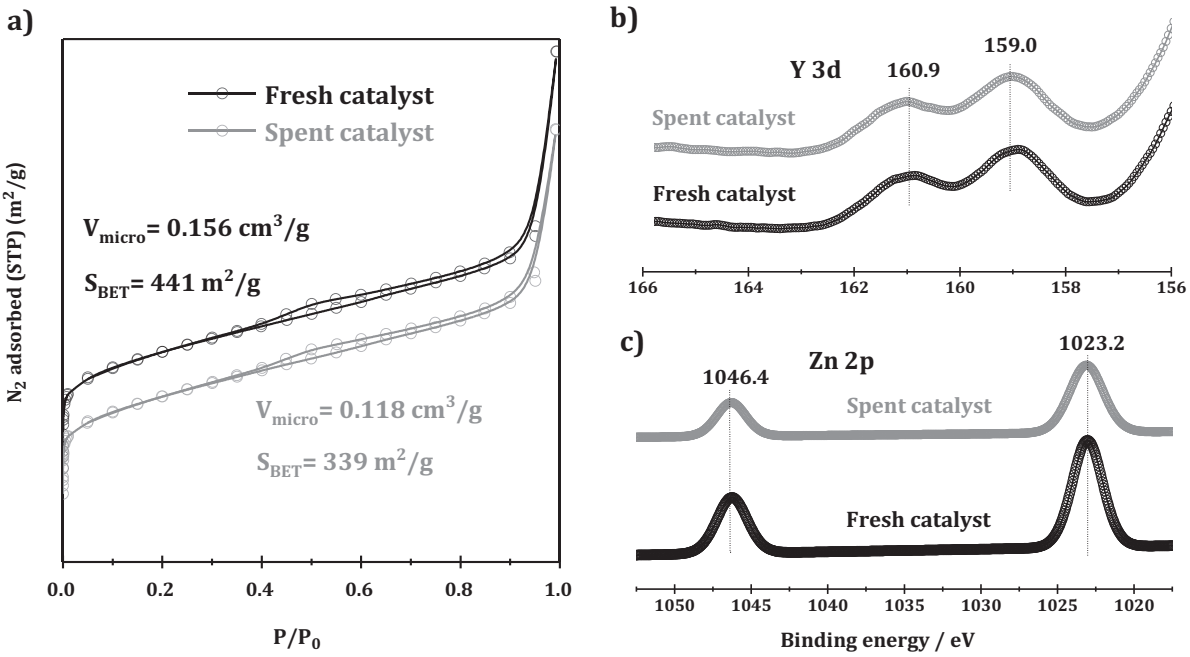

Fig. 3. N_2 absorption-desorption isotherms (a), the Y 3d (b) and Zn 2p XPS signals (c) of the fresh and spent Zn-Y/Beta catalysts obtained after the ETB conversion at 673 K for TOS = 70 h.

of the Zn states of Zn/H-ZSM-5 before and after methane dehydroaromatization [41].

Summarizing these experimental observations, we conclude that the coke compounds formed during the ETB reaction can lead to a partial blocking of pores, which causes a slight decrease in the BET surface area and micropore volume. On the other hand, the coke compounds can also cause a partial coverage of the active sites making them non-accessible for further reaction. To get more detailed information on the deactivation behaviors of the Zn-Y/Beta catalysts during the ETB conversion, the nature of the initial products, reactive intermediates and organic deposits during the catalyst lifetime were investigated by MS, *in situ* DRIFTS, UV–vis, TGA, GC–MS, and ^{13}C CP MAS NMR spectroscopy in the following sections.

3.3. On-line MS monitoring of the ETB conversion over the Zn-Y/Beta catalyst

To get more information about the initial products or intermediates formed during the ETB conversion over Zn-Y/Beta catalyst, on-line MS experiments were performed. According to the previous report of Wang and the co-workers [42], the formation of acetone was observed during the ethanol conversion over ZnO oxide and several steps are involved in this process: (i) the dehydrogenation of ethanol to acetaldehyde ($CH_3CH_2OH \rightarrow CH_3CHO + H_2$); (ii) the Aldol condensation reaction of acetaldehyde to acetaldol ($2CH_3CHO \rightarrow CH_3CHOHCH_2CHO$); (iii) the dehydrogenation of acetaldol to 3-oxobutanal ($CH_3CHOHCH_2CHO \rightarrow CH_3COCH_2CHO + H_2$); (iv) the reaction of 3-oxobutanal and water to acetone ($H_2O + CH_3COCH_2CHO \rightarrow CH_3COCH_3 + CO_2 + H_2$). In addition, acetone could also be formed via the Cannizzaro and Ketonization routes, i.e. the Cannizzaro reaction of acetaldehyde to acetates, and the Ketonization reaction of acetates to acetone [43,44]. Considering the above-mentioned intermediates and the generally accepted reaction mechanism of ETB conversion [12], the possible intermediates or products, e.g., water (m/z = 18), hydrogen (m/z = 2), acetaldehyde (m/z = 44), crotonaldehdye (m/z = 70), crotonyl alcohol (m/z = 57), butadiene (m/z = 54), acetone (m/z = 58), and acetic acid (m/z = 60) that might be formed during the initial stage of the ETB conversion were monitored by on-line MS. As shown in Fig. 4, acetaldehyde and hydrogen were first formed during the initial stage of the ETB conversion, indicating that the ethanol dehydrogenation to acetaldehyde was the first reaction step. With increasing TOS, crotonaldehdye and crotonyl alcohol appeared, followed by butadiene. These observations hinted to a cascade reaction of acetaldehyde, i.e. the aldol condensation of acetaldehyde to crotonaldehyde, the Meerwein-Ponndorf-Verley (MPV) reduction of crotonaldehyde to crotonyl alcohol, and the dehydration of crotonyl alcohol to butadiene [12]. In addition, a detectable amounts of acetone and acetic acid could be observed as the by-products. The presence of acetic acid indicated the Cannizzaro reaction of acetaldehyde, while the later appearance of acetic acid as compared with acetone excluded the pathway of acetone formation via the Cannizzaro and Ketonization routes. With

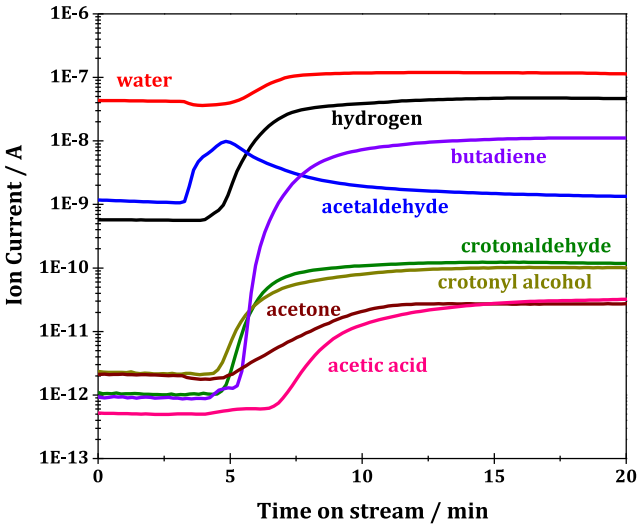

Fig. 4. On-line MS monitoring of the reaction products formed during the initial stages of the ETB conversion at 673 K for TOS up to 20 min.

the progress of the ETB conversion, acetone could be further converted to the by-product isobutene [42] or be transformed to other large unsaturated ketones together with acetaldehyde. The large unsaturated ketones acted as precursors of coke compounds, which would be discussed in the next sections.

3.4. *In situ* DRIFTS and UV–vis studies of the ETB conversion over the Zn-Y/Beta catalyst

The *in situ* DRIFTS spectra of the surface intermediates or gas-phase products formed over the Zn-Y/Beta catalyst during the ETB conversion are shown in Fig. 5. The occurrence of the negative band at 3680 cm^{-1}, immediately after starting the ethanol flow, hinted to an interaction of ethanol with Zn—OH or Y—OH groups. Another negative band at 3734 cm^{-1} due to terminal silanol groups emerged subsequently, indicating that ethanol molecules were preferentially adsorbed on the Zn—OH or Y—OH groups. According to our previous study [12], the Zn—OH and Y—OH groups were responsible for the ETB conversion, e.g. ethanol dehydrogenation and aldol condensation, while the weakly acidic Si—OH groups were responsible for the side reactions of ethanol dehydration to ethene/DEE. During ETB reaction, the bands at 1705 cm^{-1} due to acetaldehyde, and bands at 1649 and 1585 cm^{-1} due to ν(C=O) and ν(C=C) vibration modes of coupling products, e.g. crotonaldehyde and other large unsaturated aldehydes/ketones, could be observed, in good agreement with the MS results shown in Fig. 4. These observations indicated that the aldol condensation occurred immediately after the ethanol dehydrogenation. Additionally, the bands at high wavenumbers of 2875–2960 cm^{-1}, due to CH_3ν(a), CH_2ν(a), and CH_3ν(s) stretching modes of the unreacted ethanol molecules, could be observed. With the progress of the ETB conversion, bands at low wavenumbers of 1060–1280 cm^{-1} and 1448 cm^{-1} also occurred. The former bands were attributed to ethanol molecules coordinated at Lewis acid sites and ethoxy groups, while the latter one was due to acetate species [12]. With the further progress of ETB conversion, the band at 1448 cm^{-1} gradually disappeared, while the bands at 1570, 1495, and 1380 cm^{-1} appeared instead, which could be explained by the C=C ring vibrations of aromatics and C-H stretching vibrations [39]. These bands hinted to the formation of alkylated aromatics during the ETB conversion on the Zn-Y/Beta catalyst, which was further confirmed by the UV–vis and GC–MS results (vide infra).

With the progress of ETB conversion, furthermore, the intensities of the unreacted ethanol bands at 1280, 1060, and 1170 cm^{-1} started to increase, in accordance with catalyst deactivation process. Meanwhile, the bands of acetaldehyde decreased at first and then gradually increased, revealing that the acetaldehyde formed during the initial stage of the ETB conversion was rapidly involved in the subsequent aldol condensation reaction. With the occurrence of catalyst deactivation, less acetaldehyde intermediates could be converted, which was in line with the catalytic results shown in Fig. 1.

The *in situ* UV–vis spectra recorded during the ETB conversion over the Zn-Y/Beta catalyst at 673 K up to TOS = 60 h are shown in Fig. 6. During the initial stage of the ETB conversion, weak bands at 210 and 225 nm due to acetaldehyde appeared (Fig. S4), indicating the occurrence of ethanol dehydrogenation, in good agreement with the MS (Fig. 4) and *in situ* DRIFTS results (Fig. 5). With the progress of the ETB conversion, the concentration of acetaldehyde, reflected by the intensities of the characteristic UV–vis band (210 nm), decreased at first and then gradually increased. These observations indicated that acetaldehyde was rapidly involved in subsequent reactions, however, with the occurrence of catalyst deactivation much more acetaldehyde intermediates could not be further converted and, therefore, be detected by UV–vis spectroscopy, as revealed by the *in situ* DRIFTS results (Fig. 5). Simultaneously, additional bands at 245–425 nm appeared. According to our previous studies, the bands at 245, 275–285, 345, and 425 nm were assigned to dienes, monoenylic cabenium ions (e.g. cyclopentenyl and cyclohexenyl cations) or polyalkylaromatics, dienylic carbenium ions or larger unsaturated aldehydes/ketones ($n \rightarrow \pi^*$), and trienylic carbenium ions or polycyclic aromatics, respectively [45–48]. Considering the absence of Brønsted acid sites in the present Zn-Y/Beta catalysts, and the occurrence of aldol condensation and MPV reduction of the formed acetaldehyde during the ETB conversion, the coupling products, e.g., crotonaldehyde and other large unsaturated aldehydes/ketones, could also give rise to UV–vis bands at 245–345 nm ($n \rightarrow \pi^*$) (Fig. S4). Therefore, the UV–vis bands at 345 and 425 nm under study should be attributed the $n \rightarrow \pi^*$ absorption of large unsaturated aldehydes/ketones and polycyclic aromatics, respectively. With the further progress of the ETB conversion, the bands of polyalkylaromatics or the coupling products of acetaldehyde (285 nm) slighly shifted to 320–330 nm, indicating that the carbon chain growth or the occuring of cyclization reactions.

To summarize the results from the *in situ* DRIFTS and UV–vis experiments, we concluded that acetaldehyde was firstly formed and rapidly involved in a subsequent aldol condensation reaction. Thereafter, carbon chain growth and cyclization reactions occurred, and polyalkylaromatics or unsaturated aldehydes/

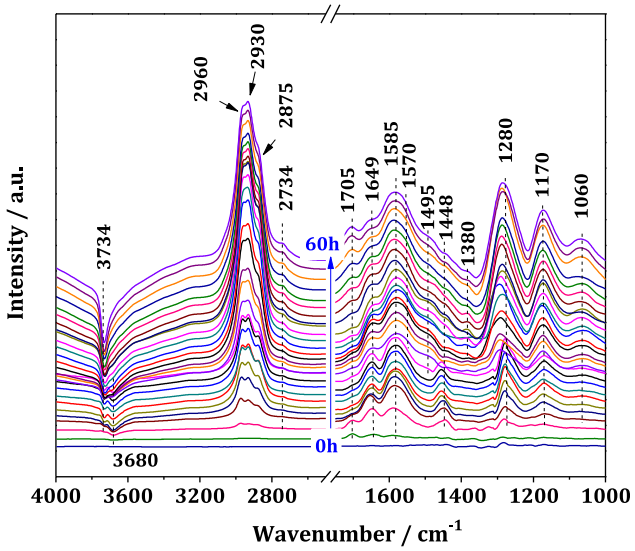

Fig. 5. *In situ* DRIFTS spectra recorded during the ETB conversion over the Zn–Y/Beta catalyst at 673 K for TOS of up to 60 h.

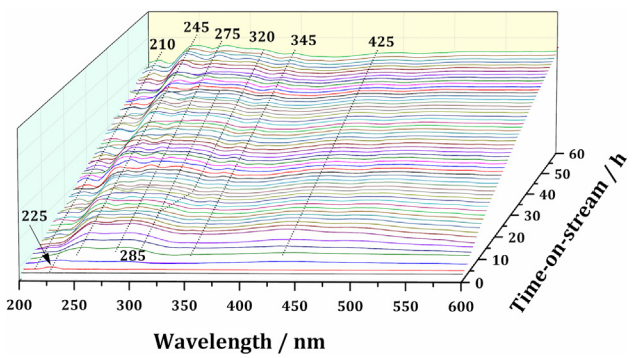

Fig. 6. *In situ* UV/vis spectra recorded during the ETB conversion over the Zn–Y/Beta catalyst at 673 K for TOS of up to 60 h.

ketones could be formed, resulting in a gradual coverage of the active sites of the Zn-Y/Beta catalyst.

3.5. TGA, GC–MS, and ^{13}C MAS NMR investigations of carbon deposits on the spent Zn-Y/Beta catalysts

To quantify the carbon deposits formed on the Zn-Y/Beta catalyst during the ETB conversion for TOS of 0.5–70 h, the weight contents of these deposits were determined by TGA in the temperature range of 298–1073 K. According to Fig. 7, two ranges of obvious weight losses could be recognized: A low-temperature weight loss (Δ_{lt}) at < 573 K and a high-temperature weight loss (Δ_{ht}) at >673 K, which were ascribed to volatile compounds and coke compounds, respectively. For the spent catalysts after the TOS of 0.5, 5.0, 10, and 20 h, a similar low-temperature (<573 K) weight loss (Δ_{lt}) of about 3.6% was determined, while the catalysts obtained after longer TOS of 30, 50 and 70 h, were characterized by a lower weight loss of about 2.8% in the same temperature range. These observations indicated that more small volatile compounds were formed with short reaction time. In the high-temperature range of 673–1073 K, the weight losses were gradually increased from 1.9 to 5.6% with the progress of the ETB conversion, indicating that the large organic compounds were gradually accumulated on the Zn-Y/Beta catalyst. In comparison with our previous studies of the coke compounds on deactivated H-SSZ-13, SAPO-34, and Ga-ZSM-5 catalysts in ethene-to-propene (ETP) and methanol-to-hydrocarbons (MTH) reactions, the lower weight losses of the deactivated Zn-Y/Beta catalyst under study indicated that pore-blocking had a minor contribution to the catalyst deactivation. On the other hand, this was similar to the deactivation of AlPO-34 catalysts with trace amounts of Brønsted acid sites applied in the MTH conversion [49,50], i.e. the coverage of the active sites by the coke compounds should be the main reason for the deactivation of the catalysts.

The chemical composition of the organic compounds occluded in the Zn-Y/Beta catalysts obtained after the ETB conversion for TOS of 0.5–70 h were determined by GC–MS and the results are shown in Fig. 8. Obviously, unsaturated aldehydes/ketones with five or six membered-rings were detected for all spent Zn-Y/Beta catalysts. The concentration and proportions of the organic deposits, reflected by the intensities of the GC signals, changed strongly with the progress of ETB conversion. Typically, 2,4-dimethyl benzaldehyde were observed as the dominant organic species occluded in the spent catalysts, even after the short TOS of 0.5 h. With increasing TOS, the amounts of 2,4-dimethyl benzaldehyde gradually increased, in good agreement with the performance of the high-temperature weight loss (Δ_{ht}) determined by TGA (Fig. 7). On the other hand, the amounts of the smaller unsaturated aldehydes/ketones, e.g. polymethylcyclopentenone and polymethylcyclohexenone, decreased instead, which also fits very well with the low-temperature weight loss (Δ_{lt}) determined by TGA. On the basis of these observations, it can be concluded that the polymethylcyclopentenone and polymethylcyclohexenone originated from the aldol condensation of acetaldehyde and/or acetone gradually transform to 2,4-dimethyl benzaldehyde. In addition, as shown in Fig. S5, the spent Zn-Y/Beta catalysts under study could be fully dissolved in HF solution and no insoluble compounds, such as black organic particles, occurred in the extract. Therefore, considering the absence of larger coke compounds, like anthracene and phenanthrene, a deactivation of the spent Zn-Y/Beta catalysts by pore blocking had a low probability, in accordance with the TGA results (Fig. 7).

The ^{13}C CP MAS NMR spectra of Zn-Y/Beta catalysts obtained after the ETB conversion for TOS = 0.5–70 h are shown in Fig. 9. For the spent catalysts after short TOS of 0.5 and 5 h, adsorbed ethanol ($\delta^{13}C$ = 58 and 17 ppm) was observed as the main organic species [51]. In addition, weak signals at 11–30, 115–149, and 185–190 ppm, attributed to the carbon atoms of alkyl groups, olefinic and aromatic compounds [49] as well as unsaturated aldehydes/ketones, i.e. 2,4-dimethyl benzaldehyde ($\delta^{13}C$ = 192, 141, 139, 133, 127 and 19 ppm) [52], respectively, could be observed. With increasing TOS, the sharp signals at 115 and 149 ppm due to carbon atoms in —CH=CH— groups of dienes or unsaturated aldehydes/ketones gradually decreased, while the signals of methylene carbon atoms (—CH_2—) in the alkyl groups of dienes or unsaturated aldehydes/ketones greatly increased instead [53]. These observations indicated that cyclization reactions occurred with increasing TOS, in good agreement with the *in situ* UV–vis results. Furthermore, the amount of aromatics, reflected by the intensities of the signals at 125–150 ppm gradually increased with the progress of the ETB conversion, which fitted well with the TGA and GC–MS results.

To summarize the results of the TGA, GC–MS, and ^{13}C CP MAS NMR investigations, we come to the conclusion that smaller

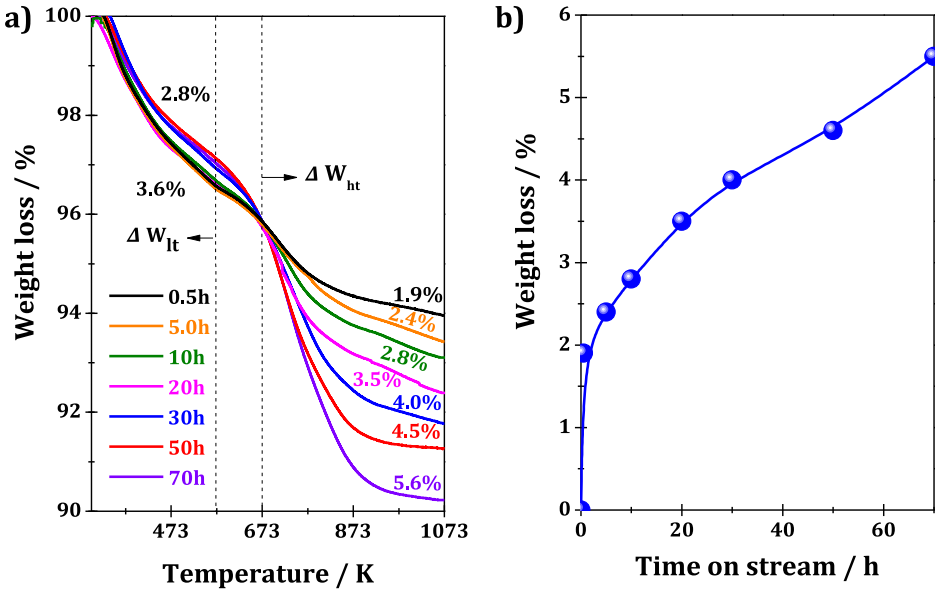

Fig. 7. TGA curves of spent Zn-Y/Beta catalysts obtained after the ETB conversion at 673 K for TOS of 0.5–70 h (a) and weight loss plotted as a function of TOS (b).

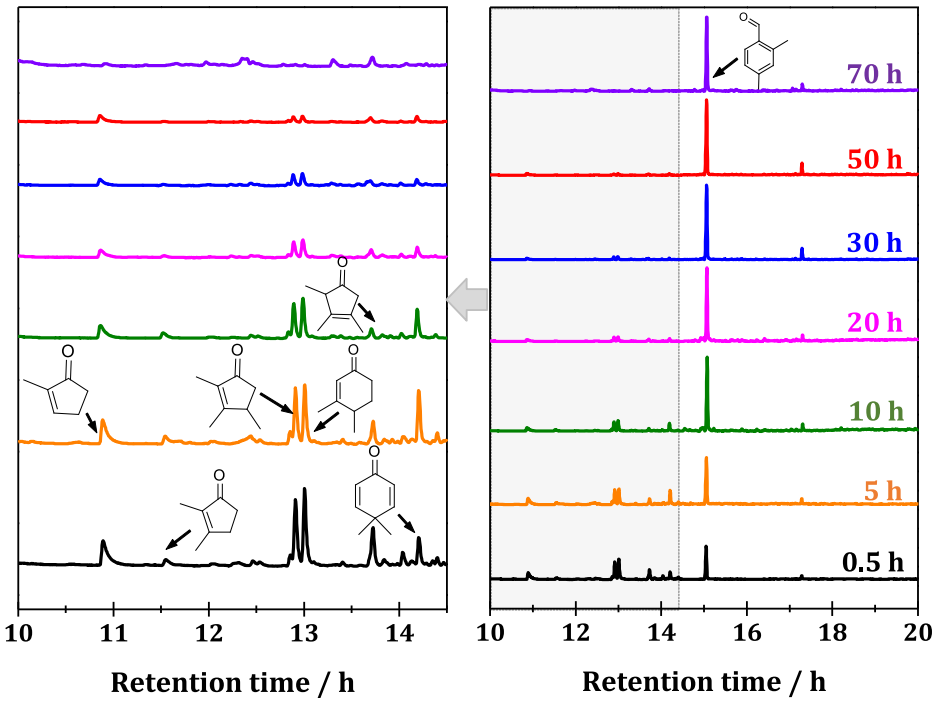

Fig. 8. GC–MS chromatograms of the organic extracts of spent Zn-Y/Beta catalysts obtained after the ETB conversion at 673 K for TOS of 0.5–70 h.

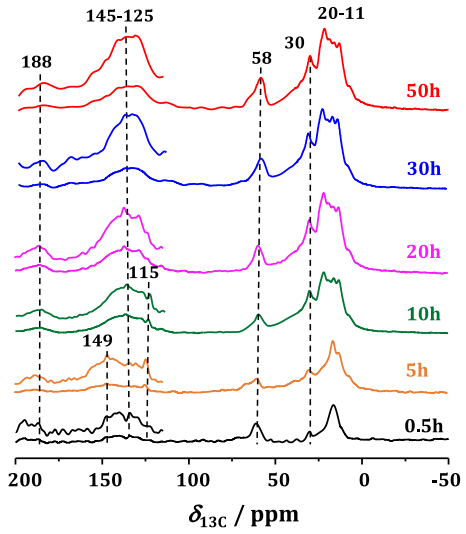

Fig. 9. ^{13}C CP MAS NMR spectra of spent Zn-Y/Beta catalysts obtained after the ETB conversion at 673 K for TOS of 0.5–50 h.

unsaturated aldehydes/ketones are formed for short TOS. These compounds are transformed to larger organic deposits, e.g. 2,4-dimethyl benzaldehyde, after longer TOS. Considering the low coke contents of the spent Zn-Y/Beta catalysts and the absence of larger coke compounds, the deactivation of the spent Zn-Y/Beta catalysts by pore blocking has a low probability.

3.6. Deactivation mechanisms of Zn-Y/Beta zeolite catalyst during the ETB conversion

Several complementary approaches applied in the present study, e.g. MS, *in situ* DRIFTS, UV–vis, TGA, GC–MS, and ^{13}C CP MAS NMR spectroscopy, can give detailed insights into the formation of organic intermediates and the reasons for the deactivation of the Zn-Y/Beta catalyst during the ETB conversion.

As demonstrated by on-line MS results, ethanol dehydrogenation to acetaldehyde is the first step of the ETB conversion, which is also supported by the *in situ* DRIFTS and UV–vis investigations. Thereafter, a cascade reaction of acetaldehyde occurs, i.e. the aldol condensation of acetaldehyde to crotonaldehyde, the Meerwein-Ponndorf-Verley (MPV) reduction of crotonaldehyde to crotonyl alcohol, and the dehydration of crotonyl alcohol to butadiene. These multistep reactions follow the well accepted mechanism of the ETB conversion shown in Scheme 1 (Path 1). Meanwhile, acetone as an intermediate can also be formed (see Fig. 4), and the side reactions containing a carbon chain growth and cyclization also occur, which are supported by the *in situ* DRIFTS, UV–vis as well as GC–MS investigations. According to the previous studies, acetaldehyde, from the ethanol dehydrogenation, is transformed to 2- and 4-methylbenzaldehyde via the sequential reaction [54,55], and acetone, from acetaldehyde, can also be transformed to larger coke compounds during the reaction [56].

Considering all the information obtained from the catalytic and spectroscopic investigations in the present work, we can summarize the deactivation mechanism of the Zn-Y/Beta catalyst during the ETB conversion, as illustrated in Scheme 1 (path 2 and 3). The main difference between path 2 and path 3 lies in the sequence of the participation of acetone in the aldol condensation. Via the self- and cross-condensation of acetaldehyde and acetone, 5-methyl-2,4,6-oct-trienal can be formed and, then, cyclized to 2,4-dimethyl benzaldehyde, according to path 2 and path 3. Simultaneously, polymethylcyclopentenone and polymethylcyclohexenone can be formed via the cyclization of the unsaturated aldehydes/ketones with different chain length, as revealed by the GC–MS results. With the progress of the ETB conversion, 2,4-dimethyl benzaldehyde is gradually accumulated and leads to a partial blocking of the pores of the Zn-Y/Beta catalyst and a gradual coverage of the Zn and Y species. However, because of the low amounts of coke compounds occluded in the deactivated Zn-Y/Beta catalysts (Fig. 7) and the small size of 2,4-dimethyl benzaldehyde in comparison with the pore sizes of zeolite Beta (0.66 nm × 0.67 nm ↔ 0.56 nm × 0.56 nm), the probability of pore blocking as a dominating reason for the deactivation of Zn-Y/Beta

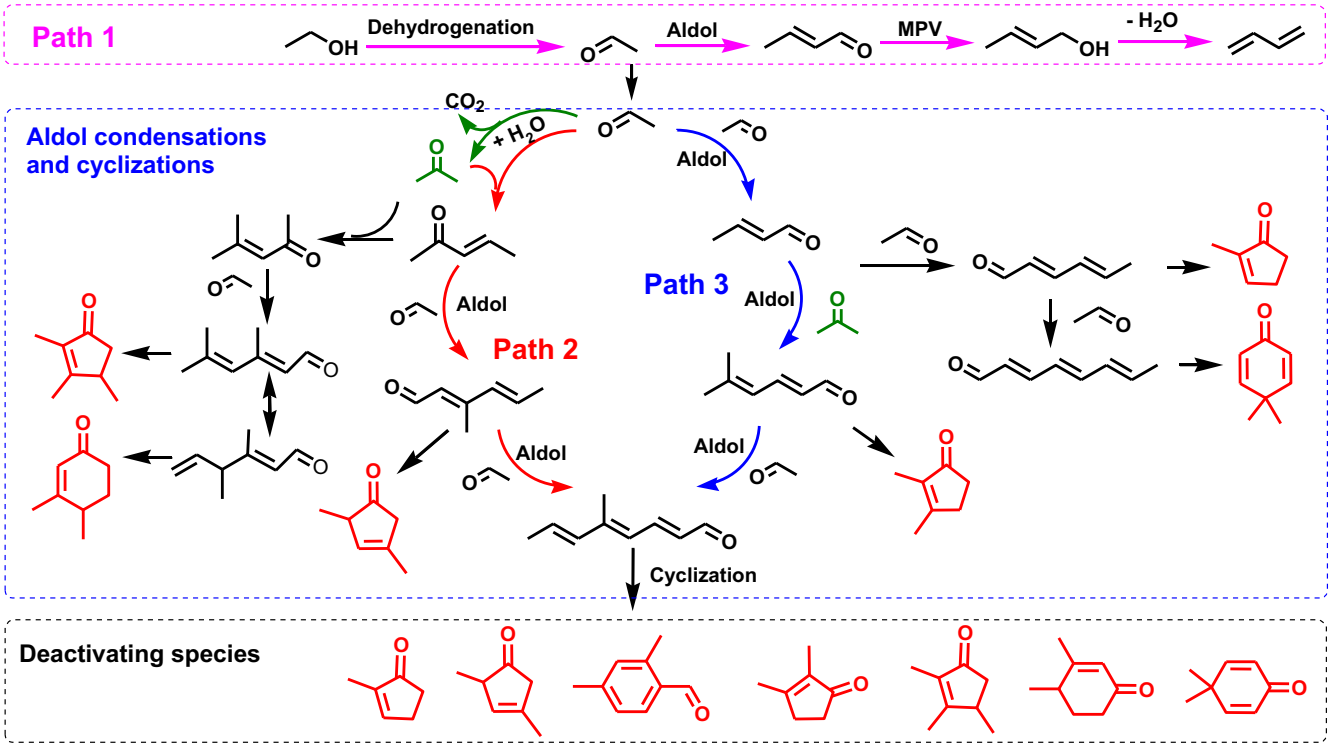

Scheme 1. Proposed reaction pathway of the ETB conversion over Zn-Y/Beta catalyst and the suggested mechanism of the catalyst deactivation.

catalyst can be excluded. On the other hand, the gradually covering the Zn and Y species by organic deposits can make these catalytically active sites non-accessible for reactant ethanol or acetaldehyde. In this case, no acetaldehyde can be further converted to butadiene and escape from the catalysts as a by-product, as supported by the catalytic results (Fig. 1). Fortunately, the deactivating species can be removed from catalyst surface via a simple calcination in the oxidizing atmosphere and the complete regeneration of Zn-Y/Beta can be realized. To improve the catalyst lifetime, the desorption of 2,4-dimethyl benzaldehyde could be enhanced by increasing the reaction temperature. Another approach could be optimizing the density of the active metal sites of the Zn-Y/Beta catalyst. In this case, the covering of all active metal sites by coke deposits should take much longer and would increase the catalyst lifetime.

4. Conclusions

In the present work, the stability and the deactivation behaviors of the Zn-Y/Beta catalyst during the ETB conversion are disclosed. To elucidate the deactivation mechanism of the catalyst during the ETB conversion, several complementary methods, such as MS, *in situ* DRIFTS, UV–vis, TGA, GC–MS, and ^{13}C CP MAS NMR spectroscopy, have been employed. On the basis of the catalytic and spectroscopic investigations, the deactivation mechanism of the Zn-Y/Beta catalyst during the ETB conversion can be summarized as follows:

(i) Acetaldehyde as the first intermediate/product formed during the initial stage of the ETB conversion is rapidly involved in a subsequent aldol condensation, which results in the formation of unsaturated aldehydes/ketones with different chain length (MS, *in situ* DRIFTS and UV–vis).

(ii) Acetone formed via the aldol condensation of acetaldehyde (on-line MS) can also be converted to larger unsaturated aldehydes/ketones via the self-condensation or cross-condensation with acetaldehyde (*in situ* UV–vis and GC–MS).

(iii) With the progress of the ETB conversion, cyclization reactions occur and polymethylcyclopentenone and polymethylcyclohexenone as well as 2,4-dimethyl benzaldehyde are formed (GC–MS, ^{13}C CP MAS NMR).

(iv) Caused by the deposition of large unsaturated aldehydes/ketones, such as 2,4-dimethyl benzaldehyde (UV–Vis, GC–MS), a gradual coverage of the catalytically acitive Zn and Y species of the Zn-Y/Beta catalyst occurs, which leads to a gradual deactivation of the ETB catalyst.

Acknowledgements

This work is supported by the National Natural Science Foundation of China (21872072, 21722303, 21421001), Municipal Natural Science Foundation of Tianjin (18JCZDJC37400), 111 project (B12015, B18030), the Fundamental Research Funds for the Central Universities (63185015) and the Foundation of China Scholarship Council (CSC).

Appendix A. Supplementary material

Supplementary data associated with this article can be found, in the online version, at https://doi.org/10.1016/j.jcat.2018.08.019.

References

[1] C. Angelici, B.M. Weckhuysen, P.C.A. Bruijnincx, Chemocatalytic conversion of ethanol into butadiene and other bulk chemicals, ChemSusChem 6 (2013) 1595–1614.

[2] J. Sun, Y. Wang, Recent advances in catalytic conversion of ethanol to chemicals, ACS Catal. 4 (2014) 1078–1090.
[3] E.V. Makshina, M. Dusselier, W. Janssens, J. Degreve, P.A. Jacobs, B.F. Sels, Review of old chemistry and new catalytic advances in the on-purpose synthesis of butadiene, Chem. Soc. Rev. 43 (2014) 7917–7953.
[4] J.V. Ochoa, C. Bandinelli, O. Vozniuk, A. Chieregato, A. Malmusi, C. Recchia, F. Cavani, An analysis of the chemical, physical and reactivity features of MgO–SiO_2 catalysts for butadiene synthesis with the Lebedev process, Green Chem. 18 (2016) 1653–1663.
[5] A.D. Patel, K. Meestters, H. Uil, E. Jong, K. Blok, M.K. Patel, Sustainability assessment of novel chemical processes at early stage: application to biobased processes, Energy Environ. Sci. 5 (2012) 8430–8444.
[6] V.L. Sushkevich, I.I. Ivanova, Mechanistic study of ethanol conversion into butadiene over silver promoted zirconia catalysts, Appl. Catal. B Environ. 215 (2017) 36–49.
[7] P. Müller, S.P. Burt, A.M. Love, W.P. McDermott, P. Wolf, I. Hermans, Mechanistic study on the Lewis acid catalyzed synthesis of 1,3-Butadiene over Ta-BEA using modulated Operando DRIFTS-MS, ACS Catal. 6 (2016) 6823–6832.
[8] Y. Hayashi, S. Akiyama, A. Miyaji, Y. Sekiguchi, Y. Sakamoto, A. Shiga, T. Koyama, K. Motokura, T. Baba, Experimental and computational studies of the roles of MgO and Zn in talc for the selective formation of 1,3-butadiene in the conversion of ethanol, Phys. Chem. Chem. Phys. 18 (2016) 25191–25209.
[9] P.I. Kyriienko, O.V. Larina, S.O. Soloviev, S.M. Orlyk, C. Calers, S. Dzwigaj, Ethanol conversion into 1,3-Butadiene by the Lebedev method over MTaSiBEA zeolites (M = Ag, Cu, Zn), ACS Sustain. Chem. Eng. 5 (2017) 2075–2083.
[10] J.L. Cheong, Y. Shao, S.J.R. Tan, X. Li, Y. Zhang, S.S. Lee, Highly active and selective Zr/MCF catalyst for production of 1,3-Butadiene from ethanol in a dual fixed bed reactor system, ACS Sustain. Chem. Eng. 4 (2016) 4887–4894.
[11] A. Chieregato, J.V. Ochoa, C. Bandinelli, G. Fornasari, F. Cavani, M. Mella, On the chemistry of ethanol on basic oxides: revising mechanisms and intermediates in the Lebedev and Guerbet reactions, ChemSusChem 8 (2015) 377–388.
[12] T. Yan, W. Dai, G. Wu, S. Lang, M. Hunger, N. Guan, L. Li, Mechanistic insights into one-step catalytic conversion of ethanol to butadiene over bifunctional Zn-Y/Beta zeolite, ACS Catal. 8 (2018) 2760–2773.
[13] W. Janssens, E.V. Makshina, P. Vanederen, F.D. Clippel, K. Houthoofd, S. Kerkhofs, J.A. Martens, P.A. Jacobs, B.F. Sels, Ternary Ag/MgO-SiO_2 Catalysts for the Conversion of ethanol into butadiene, ChemSusChem 8 (2015) 994–1008.
[14] S. Shylesh, A.A. Gokhale, C.D. Scown, D. Kim, C.R. Ho, A.T. Bell, From sugars to wheels: the conversion of ethanol to 1,3-butadiene over metal-promoted magnesia-silicate catalysts, ChemSusChem 9 (2016) 1462–1472.
[15] C. Angelici, M.E.Z. Velthoen, B.M. Weckhuysen, P.C.A. Bruijnincx, Effect of preparation method and CuO promotion in the conversion of ethanol into 1,3-butadiene over SiO_2-MgO Catalysts, ChemSusChem 7 (2014) 2505–2515.
[16] J.V. Ochoa, A. Malmusi, C. Recchi, F. Cavani, Understanding the role of gallium as a promoter of magnesium silicate catalysts for the conversion of ethanol into butadiene, ChemCatChem 9 (2017) 2128–2135.
[17] C. Angelici, M.E.Z. Velthoen, B.M. Weckhuysen, P.C.A. Bruijnincx, Influence of acid–base properties on the Lebedev ethanol-to-butadiene process catalyzed by SiO_2–MgO materials, Catal. Sci. Technol. 5 (2015) 2869–2879.
[18] C. Angelici, F. Meirer, A.M.J. Eerden, H.L. Schaink, A. Goryachev, J.P. Hofmann, E. J.M. Hensen, B.M. Weckhuysen, P.C.A. Bruijnincx, Ex situ and operando studies on the role of copper in Cu-promoted SiO_2−MgO catalysts for the Lebedev ethanol-to-butadiene process, ACS Catal. 5 (2015) 6005–6015.
[19] O. Larina, P. Kyriienko, S. Soloviev, Ethanol conversion to 1,3-butadiene on ZnO/MgO–SiO_2 catalysts: effect of ZnO content and MgO:SiO_2 ratio, Catal. Lett. 5 (2015) 1162–1168.
[20] M. Zhang, M. Gao, J. Chen, Y. Yu, Study on key step of 1,3-butadiene formation from ethanol on MgO/SiO_2, RSC Adv. 5 (2015) 25959–25966.
[21] S.D. Ros, M.D. Jones, D. Mattia, M. Schwaab, F.B. Noronha, J.C. Pinto, Modelling the effects of reaction temperature and flow rate on the conversion of ethanol to 1,3-butadiene, Appl. Catal. A Gen. 530 (2017) 37–47.
[22] Q. Zhu, B. Wang, T. Tan, Conversion of ethanol and acetaldehyde to butadiene over MgO−SiO_2 catalysts: effect of reaction parameters and interaction between MgO and SiO_2 on catalytic performance, ACS Sustain. Chem. Eng. 5 (2017) 722–733.
[23] W.E. Taifan, G. Yan, J. Baltrusaitis, Surface chemistry of MgO/SiO_2 catalysts during the ethanol catalytic conversion to 1,3-butadiene: in situ DRIFTS and DFT study, Catal. Sci. Technol. 7 (2017) 4648–4668.
[24] E.V. Makshina, W. Janssens, B.F. Sels, P.A. Jacobs, Catalytic study of the conversion of ethanol into 1,3-butadiene, Catal. Today 198 (2012) 338–344.
[25] S.D. Ros, M.D. Jones, D. Mattia, M. Schwaab, E. Barbosa-Coutinho, R.C. Rabelo-Neto, F.B. Noronha, J.C. Pinto, Microkinetic analysis of ethanol to 1,3-butadiene reactions over MgO-SiO_2 aatalysts based on characterization of experimental fluctuations, Chem. Eng. J. 308 (2016) 988–1000.
[26] S.-H. Chung, C. Angelici, S.O.M. Hinterding, M. Weingarth, M. Baldus, K. Houben, B.M. Weckhuysen, P.C.A. Bruijnincx, Role of magnesium silicates in wet-kneaded silica-magnesia catalysts for the Lebedev ethanol-to-butadiene process, ACS Catal. 6 (2016) 4034–4045.
[27] S.D. Ros, M.D. Jones, D. Mattia, J.C. Pinto, M. Schwaab, F.B. Noronha, S.A. Kondrat, T.C. Clarke, S.H. Taylor, Ethanol to 1,3-butadiene conversion by using ZrZn-containing MgO-SiO_2 systems prepared by co-precipitation and effect of catalysis acidity modification, ChemCatChem 8 (2016) 2376–2386.
[28] R. Ohnishi, T. Akimoto, K. Tanabe, Pronounced catalytic activity and selectivity of MgO-SiO_2-Na_2O for synthesis of buta-1,3-diene from ethanol, J. Chem. Soc. Chem. Commun. 22 (1985) 1613–1614.
[29] Z. Han, X. Li, M. Zhang, Z. Liu, M. Gao, Sol-gel synthesis of ZrO_2–SiO_2 catalysts for the transformation of bioethanol and acetaldehyde into 1,3-butadiene, RSC Adv. 5 (2015) 103982–103988.
[30] P.I. Kyriienko, O.V. Larina, S.O. Soloviev, S.M. Orlyk, S. Dzwigaj, High selectivity of TaSiBEA zeolite catalysts in 1,3-butadiene production from ethanol and acetaldehyde mixture, Catal. Commun. 77 (2016) 123–126.
[31] V.L. Sushkevich, I.I. Ivanova, E. Taarning, Ethanol conversion into butadiene over Zr-containing molecular sieves doped with silver, Green Chem. 17 (2015) 2552–2559.
[32] V.L. Sushkevich, I.I. Ivanova, Ag-promoted ZrBEA zeolites obtained by post-synthetic modification for conversion of ethanol to butadiene, ChemSusChem 9 (2016) 2216–2225.
[33] V.L. Sushkevich, I.I. Ivanova, V.V. Ordomsky, E. Taarning, Design of a metal-promoted oxide catalyst for the selective synthesis of butadiene from ethanol, ChemSusChem 7 (2014) 2527–2536.
[34] V.L. Sushkevich, D. Palagin, I.I. Ivanova, With open arms: open sites of ZrBEA zeolite facilitate selective synthesis of butadiene from ethanol, ACS Catal. 5 (2015) 4833–4836.
[35] M.D. Jones, C.G. Keir, C.D. Iulio, R.A.M. Robertson, C.V. Williams, D.C. Apperley, Investigations into the conversion of ethanol into 1,3-butadiene, Catal. Sci. Technol. 1 (2011) 267–272.
[36] H.J. Chae, T.W. Kim, Y.K. Moon, H.K. Kim, K.E. Jeong, C.U. Kim, S.Y. Jeong, Butadiene production from bioethanol and acetaldehyde over tantalum oxide-supported ordered mesoporous silica catalysts, Appl. Catal. B Environ. 150–151 (2014) 596–604.
[37] P. Müller, S.-C. Wang, S.P. Burt, I. Hermans, Influence of metal doping on the Lewis acid catalyzed production of butadiene from ethanol studied by using modulated operando diffuse reflectance infrared Fourier transform spectroscopy and mass spectrometry, ChemCatChem 9 (2017) 3572–3582.
[38] W. Dai, S. Zhang, Z. Yu, T. Yan, G. Wu, N. Guan, L. Li, Zeolite structural confinement effects enhance one-pot catalytic conversion of ethanol to butadiene, ACS Catal. 7 (2017) 3703–3706.
[39] W. Dai, X. Sun, B. Tang, G. Wu, L. Li, N. Guan, M. Hunger, Verifying the mechanism of the ethene-to-propene conversion on zeolite H-SSZ-13, J. Catal. 314 (2014) 10–20.
[40] W. Dai, X. Wang, G. Wu, N. Guan, M. Hunger, L. Li, Methanol-to-olefin conversion on silicoaluminophosphate catalysts: effect of Brønsted acid sites and framework structures, ACS Catal. 1 (2011) 292–299.
[41] B.S. Liu, Y. Zhang, J.F. Liu, M. Tian, F.M. Zhang, C.T. Au, A.S.-C. Cheung, Characteristic and mechanism of methane dehydroaromatization over Zn-Based/HZSM-5 catalysts under conditions of atmospheric pressure and supersonic jet expansion, J. Phys. Chem. C 115 (2011) 16954–16962.
[42] J. Sun, K. Zhu, F. Gao, C. Wang, J. Liu, C.H.F. Peden, Y. Wang, Direct conversion of bio-ethanol to isobutene on nanosized $Zn_xZr_yO_z$ mixed oxides with balanced acid base sites, J. Am. Chem. Soc. 133 (2011) 11096–11099.
[43] K.K. Ramasamy, M.A. Gerber, M. Flake, H. Zhang, Y. Wang, Conversion of biomass-derived small oxygenates over HZSM-5 and its deactivation mechanism, Green Chem. 16 (2014) 748–760.
[44] A.K.P. Mann, Z. Wu, F.C. Calaza, S.H. Overbury, Adsorption and reaction of acetaldehyde on shape-controlled CeO_2 nanocrystals: elucidation of structure-function relationships, ACS Catal. 4 (2014) 2437–2448.
[45] W. Dai, C. Wang, M. Dyballa, G. Wu, N. Guan, L. Li, Z. Xie, M. Hunger, Understanding the early stages of the methanol-to-olefin conversion on H-SAPO-34, ACS Catal. 5 (2015) 317–326.
[46] W. Dai, M. Dyballa, G. Wu, L. Li, N. Guan, M. Hunger, Intermediates and dominating reaction mechanism during the early period of the methanol-to-olefin conversion on SAPO-41, J. Phys. Chem. C 119 (2015) 2637–2645.
[47] A. Kuboyama, R. Yamazaki, S. Yabe, Y. Uehara, The $n\rightarrow\pi^*$ bands of phenyl carbonyl compounds, α-diketones, and quinones at low temperatures, Bull. Chem. Soc. Jpn. 42 (1969) 10–15.
[48] R.D. Martinez, A.A. Buitrago, N.W. Howell, C.H. Hearn, J.A. Joens, The near UV absorption spectra of several aliphatic aldehydes and ketones, Atmos. Environ. 26A (1992) 785–792.
[49] W. Dai, X. Wang, G. Wu, L. Li, N. Guan, M. Hunger, Methanol-to-olefin conversion catalyzed by low-silica AlPO-34 with traces of Brønsted acid sites: combined catalytic and spectroscopic investigations, ChemCatChem 4 (2012) 1428–1435.
[50] W. Dai, G. Cao, L. Yang, G. Wu, M. Dyballa, M. Hunger, N. Guan, L. Li, Insights into the catalytic cycle and activity of methanol-to-olefin conversion over low-silica AlPO-34 zeolites with controllable Brønsted acid density, Catal. Sci. Technol. 7 (2017) 607–618.
[51] S. Radhakrishnan, P.-J. Goossens, P.C.M.M. Magusin, S.P. Sree, C. Detavernier, E. Breynaert, C. Martineau, F. Taulelle, J.A. Martens, In situ solid-state ^{13}C NMR observation of pore mouth catalysis in etherification of β-Citronellene with ethanol on zeolite Beta, J. Am. Chem. Soc. 138 (2016) 2802–2808.
[52] C NMR, Version 1.1, Advanced Chemistry Development Inc., USA, 1995.
[53] W. Dai, G. Wu, L. Li, N. Guan, M. Hunger, Mechanisms of the deactivation of SAPO-34 materials with different crystal sizes applied as MTO catalysts, ACS Catal. 3 (2013) 588–596.
[54] T. Moteki, A.T. Rowley, D.T. Bregante, D.W. Flaherty, Formation pathways toward 2- and 4-methylbenzaldehyde via sequential reactions from acetaldehyde over hydroxyapatite catalyst, ChemCatChem 9 (2017) 1–10.
[55] T. Moteki, A.T. Rowley, D.W. Flaherty, Self-terminated cascade reactions that produce methylbenzaldehydes from ethanol, ACS Catal. 6 (2016) 7278–7282.
[56] B. Zhang, X. Tang, Y. Li, W. Cai, Y. Xu, W. Shen, Steam reforming of bio-ethanol for the production of hydrogen over ceria-supported Co, Ir and Ni catalysts, Catal. Commun. 7 (2006) 367–372.